Why inverted flags flap: An experimental study

Mohammad Tavallaeinejad, Michael Païdoussis, Manuel Flores Salinas, Mathias Legrand, Mojtaba Kheiri, Ruxandra Mihaela Botez

Why inverted flags flap: An experimental study

Mohammad Tavallaeinejad[1], Michael P. Païdoussis[1], Manuel Flores Salinas[2], Mathias Legrand[1], Mojtaba Kheiri[3], and Ruxandra Mihaela Botez[2]

[1] *Department of Mechanical Engineering, McGill University, Montréal, Québec, Canada*
[2] *Ecole de Technologie Supérieure, Montréal, Québec, Canada*
[3] *FSI & Aeroelasticity Laboratory, Concordia University, Montréal, Québec, Canada*

Corresponding author: mohammad.tavallaeinejad@mail.mcgill.ca

Abstract

The experiments described in this paper aim to examine the global dynamics of inverted flags and to explore the impact of periodic vortex shedding from the leading and trailing edges thereon. The effect of vortex shedding from both leading and trailing edges was investigated. It is shown that suppression of the leading and trailing edge vortices, and also inhibition of the interaction between the two counter-rotating vortices (if they exist), resulted in relatively small quantitative changes in the critical flow velocity, amplitude and frequency; but, the overall dynamics of the system remain intact. More importantly, the large-amplitude flapping persisted for all flags tested in the experiments.

Force measurements provide some insights into the relationship between vortex shedding and large-amplitude flapping; a difference between the dominant frequency of the lift and that of flapping was observed for some cases. Moreover, for heavier inverted flags, additional peaks appear in the frequency spectrum of the lift signal, with amplitudes comparable to that matching the dominant frequency of flapping.

The experimental results suggest that *fluidelastic instability* is the underlying mechanism for the flapping motion of heavy inverted flags. The near-identical qualitative behaviour of normal inverted flags and serrated ones with a splitter plate at the trailing edge suggests that the global (or qualitative) dynamics of heavy inverted flags is independent of unsteady vortex shedding from the leading and trailing edges; i.e., periodic vortex shedding is not the cause but an effect of large-amplitude flapping.

Keyword: fluid-structure interactions, inverted flags, large-amplitude flapping, fluidelastic instability, flutter

1 Introduction

This paper focuses the fluid-structure interaction (FSI) of a flexible thin plate in axial flow: a cantilevered thin plate (or flag) of length L and height H subjected to a fluid flowing axially with velocity U and directed from the free end towards the clamped one, otherwise known as an 'inverted flag;' see figure 1.

Inverted flags are known to exhibit large-amplitude periodic flapping around the undeflected equilibrium. A number of studies on the dynamics of inverted flags suggest that the physical

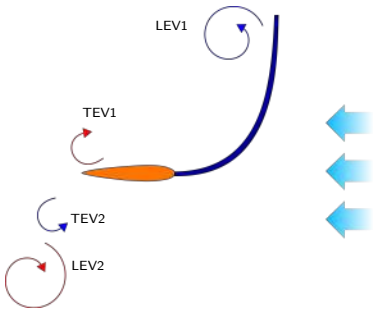

Figure 1 – Inverted flag in large-amplitude regime, shedding leading-edge vortices (LEV) and trailing-edge vortices (TEV) in the wake.

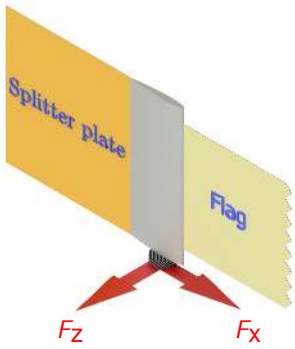

Figure 2 – Experimental set-up for a serrated inverted flag with the rigid splitter plate, showing the measured forces at the flagpole, utilizing a force balance.

mechanism underlying large-amplitude flapping may be *Vortex-Induced Vibration* (VIV) (e.g., Sader et al. 2016). In these studies, the flapping phenomenon is attributed to the periodic formation and synchronized shedding of trailing-edge vortices (TEV) and leading-edge vortices (LEV), which is a characteristic of VIV (see figure 1).

Although several aspects of the dynamics may be explained through the VIV mechanism, there are some circumstances where vortex shedding, which plays a central role in VIV, may not occur for a flapping inverted flag, hence posing a challenge to the credence of the VIV mechanism. For instance, in an experimental study, Pazhani and Acharya (2019) investigated the effect of leading-edge serrations. They found that the serrated flag *does* display large-amplitude flapping, even though vortex formation and shedding from the leading edge was not observed. Moreover, via a scaling analysis, Sader et al. (2016) predicted that VIV cannot occur for heavy flags or small mass ratios[1], yet large-amplitude flapping does. Goza et al. (2018) explored computationally the physical mechanisms for large-amplitude flapping of inverted flags, concluding that for a specific set of system parameters, large-amplitude flapping cannot be attributed to classical VIV, and also for small-amplitude flapping. Finally, Gurugubelli and Jaiman (2019) performed simulations in which a rigid splitter plate was attached to the flag trailing edge, thus suppressing trailing-edge vortex shedding; they found that inverted flags undergo large-amplitude flapping even though the interactions between vortices detached from the leading-edge at the cycle extremities were eliminated – a prediction not yet verified experimentally, which is one of the objectives of the present experiments.

The primary purpose of experiments described in this paper is to explore the correlation between vortex shedding and the flapping mechanism; specifically, the qualitative and quantitative effects of suppression of both LEV and TEV on the onset, frequency, and amplitude of flapping.

The paper is organized as follows. First, experiments with a rigid splitter plate attached to the trailing-edge of the inverted flag are described (see Figure 2), aiming to evaluate the importance of the existence of TEV and to examine the effects of forced disconnection between counter-rotating LEV on large-amplitude flapping. Second, experiments with inverted flags with

[1]The fluid-to-plate mass ratio is defined as $\mu = \rho_f L/\rho_p h$; ρ_f and ρ_p being the mass density of the fluid and plate, respectively, and h is the thickness of the plate. Small μ is associated with "heavy flags".

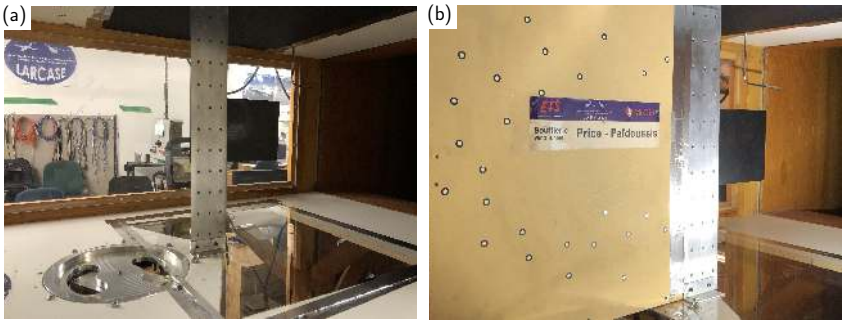

Figure 3 – Experimental set-up for the inverted flag (a) without and (b) with the rigid splitter plate.

a serrated leading-edge, similar to those used by Pazhani and Acharya (2019), are described. These experiments explore the effects of simultaneous suppression of LEV and TEV. Finally, the synchronization of lift and displacement and phase dynamics are studied.

2 Rigid splitter plate

The experiments were conducted in a subsonic wind tunnel with a fairly large test-section. The flow velocity in the test-section was incremented in small steps, and the flag motion was recorded via a high-speed camera at each step. An image processing technique was then utilized to extract the time history of oscillations. Brass plates, i.e. 'flags' ($H = 101\,\text{mm}$, $L = 198\,\text{mm}$, and thickness $h = 0.38\,\text{mm}$), as well as polycarbonate flags with different dimensions (see Table 1) were used in the experiments. Experiments have been conducted with and without a rigid splitter plate. The splitter plate was made from a plywood sheet of thickness $h_s = 10\,\text{mm}$, height $H_s = 610\,\text{mm}$, and length $L_s = 1800\,\text{mm}$, and was secured firmly to the walls of the test-section (see figure 3); no significant motion of the splitter plate was observed during the experiment, even at very high wind speeds.

Figure 4(a) shows bifurcation diagrams for the tip rotation of 160×160 mm polycarbonate flags C (circles) and flag D (diamonds), with the rigid splitter plate (filled symbols) and without it (empty symbols). A slight reduction is seen for the flapping amplitude of the flag with a splitter plate. This may be explained using observations made by Gurugubelli and Jaiman (2019). In their computational study, the inverted flag with the splitter plate exhibits only two counter-rotating vortices shed from the leading edge over the flapping cycle. The absence of the trailing edge vortices, and the inhibition of vortex-vortex interaction leads to a larger pressure distribution at the trailing edge and to a slightly smaller drag at the leading edge. This results in a smaller bending moment, which in turn leads to a reduction in the curvature along the flag.

The frequency of oscillation is also reduced slightly when the splitter plate is introduced, see Figure 4(b). For instance, the maximum reduction in flapping frequency for the $h = 1.02\,\text{mm}$ flag is at $U \backsimeq 20\,\text{m/s}$, where the frequency is reduced by almost 8%. This may also be associated with loss of the trailing edge vortices, caused by the rigid splitter plate. More specifically, the trailing edge vortex formation and shedding accelerates the drop in the pressure distribution over the flag, which consequently leads to a faster transition from maximum deflection from one side to the other, hence to a higher frequency (see Gurugubelli and Jaiman (2019)).

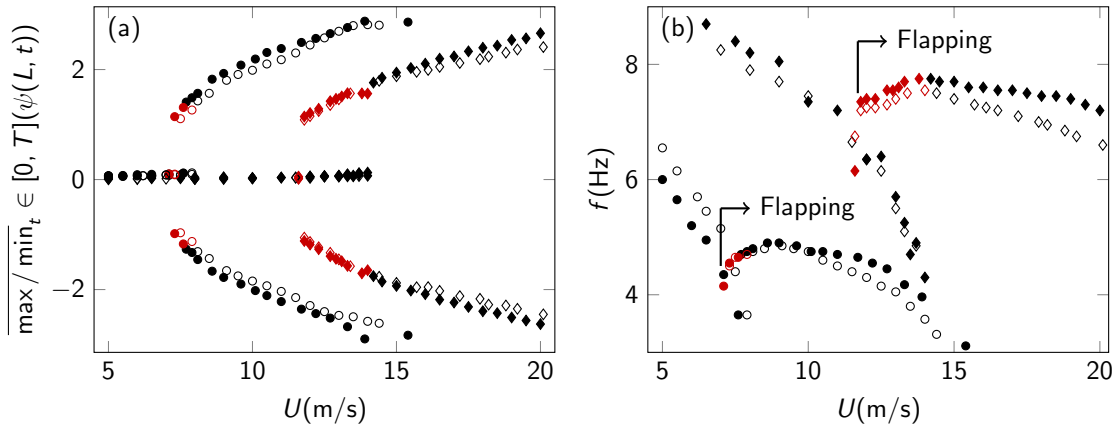

Figure 4 – Experimental results for inverted flags with $L = H = 160\,\text{mm}$ and [●] $h = 0.76\,\text{mm}$, [♦] $h = 1.02\,\text{mm}$; (a) bifurcation diagram (b) variation of the dominant frequency in PSD with the flow speed. The empty and filled markers correspond to the flags with and without the splitter plate, respectively; the black and red symbols correspond to the wind speed sweep up and down, respectively.

Figure 5 shows that the onset of large-amplitude flapping for all flags tested (except for flag B) is delayed when the splitter plate is added. This may be linked to the pressure reduction close to the leading edge of the inverted flag due to the splitter plate: the presence of the splitter plate introduces a small additional damping to the dynamical system; consequently, the critical flow velocity for large-amplitude flapping increases, and the flapping amplitude and frequency become smaller at the onset of large-amplitude flapping.

However, all these differences are very minimal. The main and most significant conclusion is that introducing a splitter plate has a minimal influence on the critical flow velocity for large-amplitude flapping, its amplitude and frequency.

Flag	Material	$L \times H$(mm)	h(mm)
A	Polycarbonate	150×225	1.02
B	Polycarbonate	150×600	0.76
C	Polycarbonate	160×160	0.76
D	Polycarbonate	160×160	1.02
E	Brass	198×101	0.38

Table 1 – Labels and dimensions of pairs of inverted flags tested in experiments with and without the rigid splitter plate.

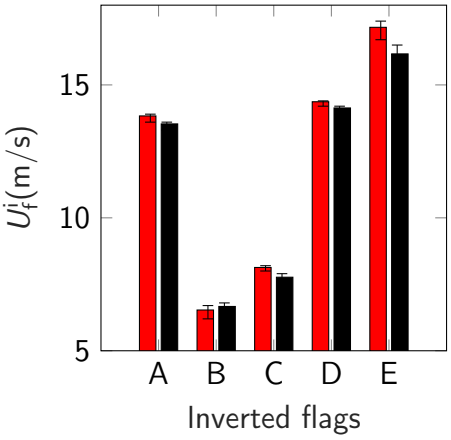

Figure 5 – Critical flow speed for the onset of large-amplitude flapping of different inverted flags with sweeping up the wind speed; [■] with and [■] without the rigid splitter plate.

3 Serrated inverted flags

In order to further understand the effect of vortex shedding on the global dynamics of inverted flags, a serrated leading-edge geometry (chevron) with height $H_s = 10\,\text{mm}$ and width $W_s = 10\,\text{mm}$ was introduced to polycarbonate flags of different aspect ratios, see Figure 6(a).

Using flow visualization techniques, Pazhani and Acharya (2019) have shown that this serrated geometry produces small counter-rotating pairs of vortices, which suppresses the formation and periodic shedding of vortices from the leading edge.

The Pazhani and Acharya (2019) experiments with serrated flags have been repeated in the present study, with wider flags – to minimize three-dimensionality of the flow caused by the side edges – also introducing a rigid splitter plate at the trailing edge of the flag to interrupt the communication of the separated shear layers. Mainly, qualitative experiments were conducted. Insofar as the onset and amplitude of large-amplitude flapping is concerned, the responses are similar to those of normal inverted flags. For instance, the experimental results for flags of $\mathcal{AR} = 3.0$ in figure 6(b) show no notable differences in the critical values of flow velocity and the amplitude of oscillation, with and without the splitter plate and serrations.

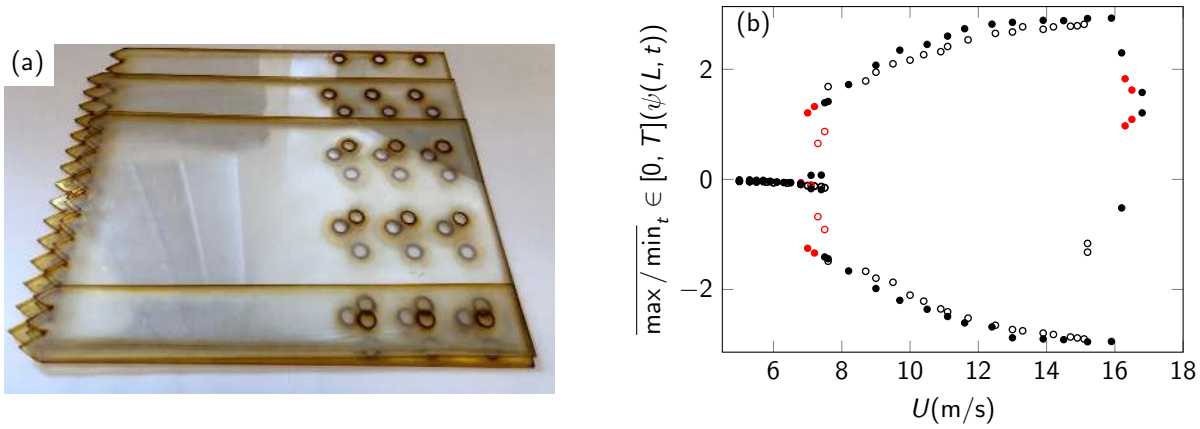

Figure 6 – Experiments with serrated inverted flags: (a) specimens used in the experiments with a similar serration geometry but different flag dimensions, (b) bifurcation diagram for an inverted flag with flat leading edge and no splitter plate (filled circles) and a serrated flag with the splitter plate at the trailing edge (empty circles); both flags are of $\mathcal{AR} = 3.0$. The black and red symbols correspond to the wind speed sweep up and down, respectively.

The observed behaviour shows that, for the range of parameters investigated in these experiments, the dynamical characteristics of inverted flags are not very sensitive to (i) the formation and periodic shedding of vortices from the leading and trailing edges, and (ii) vortex-vortex interaction (if any exists). Hence, another mechanism must be the cause of large-amplitude flapping; namely, it may be a fluidelastic *self-excited flutter*.

4 Synchronization of lift and displacement and phase dynamics

Several experiments were conducted to measure simultaneously the forces acting on the flag (i.e. lift and drag) and its motion. The phase difference between the time traces of the fluid

Table 2 – Stainless-steel inverted flags with $H = 75\,\text{mm}$, $h = 0.08\,\text{mm}$, and varying length utilized in experiments.

Flag	L(mm)	μ	$\mathcal{AR}$
A	100	0.21	0.75
B	70	0.15	1.07
C	50	0.10	1.50
D	35	0.07	2.14

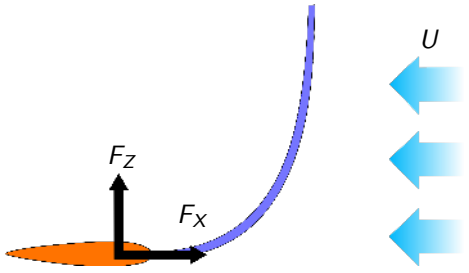

Figure 7 – Measured forces at the flagpole, utilizing a force balance.

forces and flag displacements were examined. Moreover, the dominant frequencies of the fluid forces were obtained.

These experiments were motivated by the observation made by Goza et al. (2018) for large-amplitude flapping of heavy inverted flags. They reported that, compared to light flags, several additional vortices are shed per cycle for heavy (low μ) ones, resulting in additional peaks in the frequency spectrum of the lift signal. Moreover, the frequency associated with the largest peak in the lift spectrum was different from that of the displacement spectrum. This led Goza (2019) to refer to the large-amplitude flapping of massive flags as "not-classical VIV".

In order to investigate experimentally the existence of synchronization between the lift force and displacement for heavy inverted flags, stainless steel flags of varying length (hence, varying mass ratio) were tested (see Table 2). The transverse (lift) and streamwise (drag) components of the fluid flow force were simultaneously measured at the flagpole, utilizing an in-house built aerodynamic balance (A Mini45-E Array Technology Incorporated Inc). Time traces of the lift, $F_Z(0,t)$, and the drag, $F_X(0,t)$, components (see Figure 7) were collected at 1000 Hz; the sampling rate for the tip transverse displacement, $w(L,t)$, was $160 - 280\,\text{Hz}$.

4.1 Frequency characteristics

Figure 8 shows the time traces and PSDs of $w(L,t)$ and the lift signals for a stainless-steel inverted flag with $L = 100\,\text{mm}$. In the PSD plots for the lift signal, the peaks are labeled sequentially as f_{L1}, f_{L2} etc. from lower to higher frequencies. As seen from figures 8(b,d), higher harmonics of nearly the same magnitude as the main frequency, f_1, appear in the PSD of the lift, while the motion is periodic, supporting the Goza et al. observations discussed above. By increasing the flow velocity, motion becomes chaotic-like at $U = 8.3\,\text{m/s}$; the loss of synchronization with departure from a periodic behaviour can be seen in figures 8(e,f).

The spectrograms of the displacement and lift signals are presented in figures 8 (g) and (h), respectively, showing an increase in dynamic activity and the presence of additional frequency peaks in the lift dynamics with increasing U. The increase in number and the strength of higher harmonics in the lift frequency spectrum suggests that the conjectured VIV-associated oscillation is gradually replaced by another mechanism.

Figure 9 shows the time traces and PSDs for flags with (a,b) $L = 70\,\text{mm}$, (c,d) $L = 50\,\text{mm}$, and (e,f) $L = 35\,\text{mm}$, respectively. Strikingly, the PSDs of lift and displacement show the same frequency peaks (i.e., $f_{L1} = f_1$), with the lift showing harmonics nearly equal or larger than the dominant frequency of the motion. For example, the frequency associated with the dominant

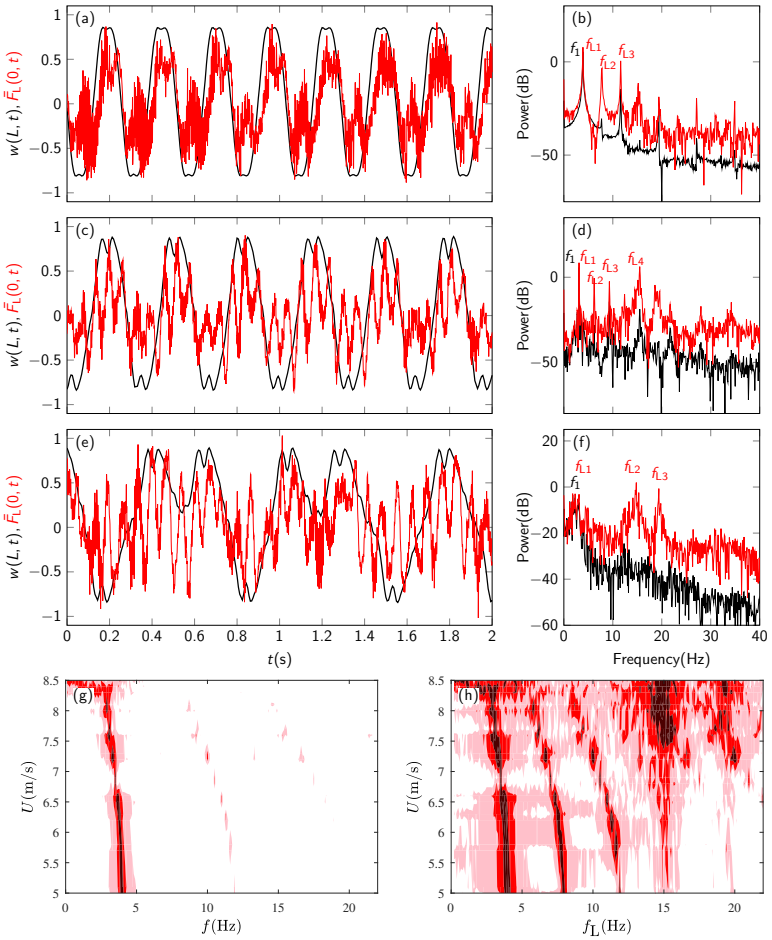

Figure 8 – (a,c,e) tip transverse displacement [—] and the normalized lift [—] at $U = 5.7\,\mathrm{m/s}$, $U = 7.7\,\mathrm{m/s}$, and $U = 8.3\,\mathrm{m/s}$; (b,d,f) associated PSDs for a stainless-steel inverted flag with $L = 100\,\mathrm{mm}$; (g-h) experimental spectrograms for the flag motion and lift, respectively – the magnitude of the power spectrum is measured in dB.

peak in the displacement PSD plot shown in figure 9(d) for $L = 50\,\mathrm{mm}$ flag at $U = 14.4\,\mathrm{m/s}$ is $f_1 = 18\,\mathrm{Hz}$, while the dominant peak in the lift PSD plot occurs at $f_{L2} = 2f_1 = 36\,\mathrm{Hz}$, and subdominant peaks occur at $f_{L1} = f_1 = 18\,\mathrm{Hz}$, $f_{L3} = 3f_1 = 54\,\mathrm{Hz}$, and $f_{L4} = 5f_1 = 90\,\mathrm{Hz}$, whereas the contribution of these harmonics in the flag oscillation is very weak. This indicates that vortex shedding may be synchronized to a higher displacement frequency; in the present case, the vortex shedding frequency is twice the flapping frequency, giving rise to a 1:2 synchronization.

4.2 Phase dynamics

It is known that in the case of VIV-driven motion of a circular cylinder in cross-flow, sharp changes occur in the phase angle between the fluid forces and cylinder motion at resonance, as the flow velocity is varied. In particular, the phase between the cross-flow force and the transverse displacement of the cylinder jumps from near 0 to near π (refer to Khalak and

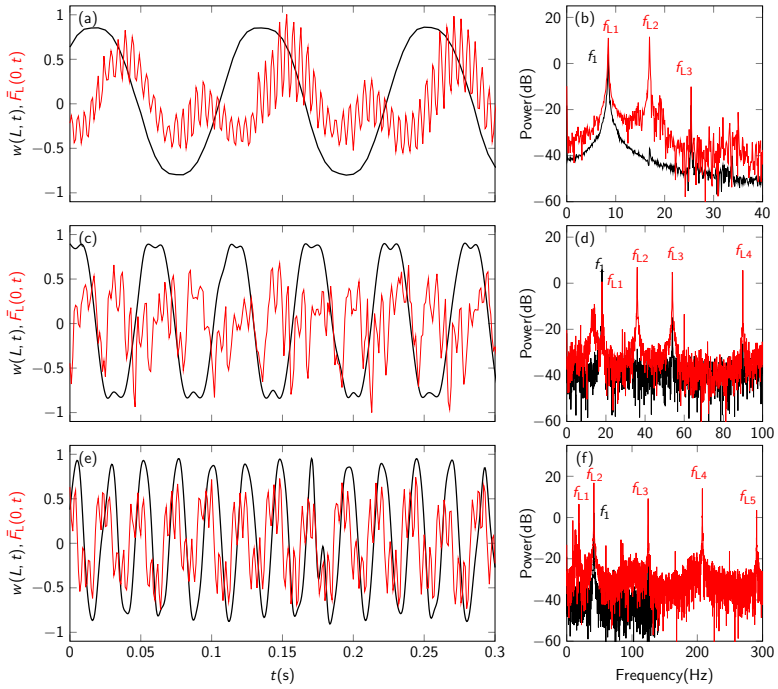

Figure 9 – (Left) tip transverse displacement [—] and the normalized lift [—] for stainless-steel inverted flags with (a) $L = 70\,\text{mm}$ at $U = 7.4\,\text{m/s}$, with (c) $L = 50\,\text{mm}$ at $U = 14.4\,\text{m/s}$, and with (e) $L = 35\,\text{mm}$ at $U = 19.0\,\text{m/s}$; (right) their associated PSDs.

Williamson 1999, Zhao et al. 2014, Seyed-Aghazadeh et al. 2017).

Here, the instantaneous phase difference between the time series obtained for the transverse displacement of the flag and the lift are calculated using the Hilbert transform (Khalak and Williamson 1999, Konstantinidis et al. 2019). The instantaneous phase is defined as $\phi_w(t) = \text{atan}[w(L,t)/\hat{w}(L,t)]$ and $\phi_F(t) = \text{atan}[F_L(0,t)/\hat{F}_L(0,t)]$, where $\hat{w}(L,t)$ and $\hat{F}_L(0,t)$ are the Hilbert transforms of $w(L,t)$ and $F_L(0,t)$, respectively. Next, the instantaneous phase lag, $\phi_d(t)$, between the lift and the displacement is calculated as $\phi_d(t) = \phi_F(t) - \phi_w(t)$.

Figure 10 shows the variation of the time-averaged phase lag, denoted by ϕ_d, as a function of the dimensionless flow velocity for flags A-D (table 2). In all cases, the time-averaged phase difference never crosses 90° and remains bounded in the [0 50] range over the large-amplitude flapping regime. The different values of the phase difference may well be due to the effect of different values of structural damping for the different flags. Similar observations have been made by Seyed-Aghazadeh et al. (2017) for triangular prisms in cross-flow, reporting that the jump from ~ 0 to $\sim 180°$ in phase difference between flow forces and the body motion did not occur, and hence the oscillation was concluded to be of the galloping type.

The above observations suggest that flag motion and vortex shedding influence each other reciprocally; however, vortex shedding does not appear to be the cause for flapping. The large-amplitude flapping of short inverted flags accompanied by high-frequency vortex shedding suggests that a *fluidelastic excitation* mechanism may be involved, and hence time-averaged aerodynamic forces govern the motion. A similar conclusion has been reached for slender prismatic bodies with bluff cross-section and sufficiently long afterbody by Nemes et al. (2012), Zhao et al. (2014) and Seyed-Aghazadeh et al. (2017), among others.

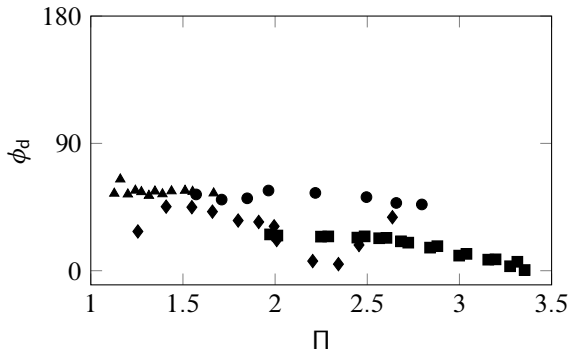

Figure 10 – Phase difference between transverse force (lift) and transverse displacement for stainless steel inverted flags with [■] $L = 100\,\text{mm}$, [●] $L = 70\,\text{mm}$, [♦] $L = 50\,\text{mm}$, and [▲] $L = 35\,\text{mm}$ over the periodic large-amplitude flapping regime.

Additionally, these observations agree well with computational predictions of Goza et al. (2018), reporting that the dominant frequency of lift (largest peak in the PSD plot) is higher than that of the tip displacement, suggesting that the motion is not "classical VIV".

5 Conclusions

Some experiments were described in this paper, aiming at examining the global dynamics of inverted flags and, in particular, at probing the impact of periodic vortex shedding from the leading and trailing edges thereon.

The effect of vortex shedding from both leading and trailing edges was investigated. It was shown that suppression of the leading and trailing edge vortices, and also inhibition of the interaction between the two counter-rotating vortices (if any exists), results in only minor changes in the critical velocity, amplitude and frequency. The overall dynamics and features of the system remained intact, and the large-amplitude flapping persisted for all flags tested in the experiments, with TEV and LEV present or suppressed.

Force measurements provided some insights into the relationship between vortex shedding and large-amplitude flapping; a difference between the dominant (peak) frequencies of the lift and flapping was found in some cases. Moreover, it was shown that for heavier inverted flags, additional frequency peaks appear in the lift frequency spectrum, with power as great as or larger than that matching the motion dominant frequency. In addition, the lift and tip displacements were found to be desynchronised in the chaotic-like flow regime for lighter flags.

The experimental results presented in Sections 2-4 suggest that a *fluidelastic instability* may be the underlying mechanism for the flapping motion of heavy inverted flags. The near-identical qualitative behaviour of normal inverted flags and those with a serrated leading edge and a splitter plate at the trailing edge suggests that the global (qualitative) dynamical characteristics of heavy inverted flags are not governed by the unsteady vortex shedding from the leading and trailing edges. In other words, periodic vortex shedding is not the cause, but an effect of large-amplitude flapping.

It is stressed that flow visualization was not carried out in the experiments with serrated flags and the splitter plate. The wake behind the flag may display three-dimensional characteristics;

yet, as reported by Pazhani and Acharya (2019), the dominant vortical features in the near wake is broken down and the coherent formation and shedding of vortices is disrupted.

There are definitely potential connections, yet to be discovered in the future, between the phase dynamics and the underlying mechanism for large-amplitude flapping. Further investigations would be desirable to better clarify the distinction between VIV and the underlying mechanism for large-amplitude flapping of heavy flags.

Acknowledgements

The financial support by the Natural Sciences and Engineering Research Council of Canada, the Solution Mining Research Institute (SMRI) and Pipeline Research Council International (PRCI) is gratefully acknowledged.

References

A. Goza. Private communication (November). 2019.

A. Goza, T. Colonius, and J. E. Sader. Global modes and nonlinear analysis of inverted-flag flapping. *Journal of Fluid Mechanics*, 857:312–344, 2018.

P. S. Gurugubelli and R. K. Jaiman. Large amplitude flapping of an inverted elastic foil in uniform flow with spanwise periodicity. *Journal of Fluids and Structures*, 90:139–163, 2019.

A. Khalak and C. H. Williamson. Motions, forces and mode transitions in vortex-induced vibrations at low mass-damping. *Journal of Fluids and Structures*, 13(7-8):813–851, 1999.

E. Konstantinidis, J. Zhao, D. L. Jacono, J. Leontini, and J. Sheridan. Phase dynamics of effective drag and lift in vortex-induced vibration at low mass-damping. *Preprint*, 2019. arXiv:1906.07375.

A. Nemes, J. Zhao, D. L. Jacono, and J. Sheridan. The interaction between flow-induced vibration mechanisms of a square cylinder with varying angles of attack. *Journal of Fluid Mechanics*, 710:102–130, 2012.

K. M. Pazhani and S. Acharya. An experimental investigation of the dynamics of an inverted serrated flag. In *AIAA Scitech 2019 Forum*, page 1891, 2019.

J. E. Sader, J. Cossé, D. Kim, B. Fan, and M. Gharib. Large-amplitude flapping of an inverted flag in a uniform steady flow – a vortex-induced vibration. *Journal of Fluid Mechanics*, 793: 524–555, 2016.

B. Seyed-Aghazadeh, D. W. Carlson, and Y. Modarres-Sadeghi. Vortex-induced vibration and galloping of prisms with triangular cross-sections. *Journal of Fluid Mechanics*, 817:590–618, 2017.

J. Zhao, J. Leontini, D. Lo Jacono, and J. Sheridan. Fluid–structure interaction of a square cylinder at different angles of attack. *Journal of Fluid Mechanics*, 747:688–721, 2014.